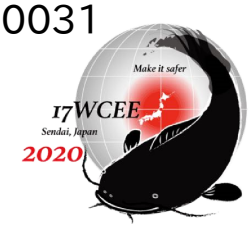

17th World Conference on Earthquake Engineering, 17WCEE
Sendai, Japan - September 13th to 18th 2020

FULL-RANGE ELASTIC-PLASTIC ANALYSIS OF CONCRETE-FILLED CIRCULAR STEEL TUBE UNDER UNIAXIAL COMPRESSION

R. Han [1], H. Zhao [2], W. Yuan [3], Z. Liu [4], S. Zhao [5], Y. Sun [6]

[1] *Ph.D. student, School of Civil Engineering, Southwest Jiaotong University, China, hanrui9201@hotmail.com*
State Key Laboratory of Geohazard Prevention and Geoenvironment Protection, Chengdu University of Technology, China
[2] *Associate Professor, State Key Laboratory of Geohazard Prevention and Geoenvironment Protection, Chengdu University of Technology, China, zhaohua@cdut.edu.cn*
[3] *Lecturer, State Key Laboratory of Geohazard Prevention and Geoenvironment Protection, Chengdu University of Technology, China, yuanweiguang19@cdut.edu.cn*
[4] *Ph.D. student, School of Civil Engineering, Southwest Jiaotong University, China, lzh0931@163.com*
[5] *Professor, School of Civil Engineering, Southwest Jiaotong University, China, zhaosc1961@163.com*
[6] *Professor, Graduate School of Engineering, Kobe University, Japan, sun@person.kobe-u.ac.jp*
China-Japan Resilient and Sustainable Concrete Structures Research Center, Southwest Jiaotong University, China

Abstract

To investigate the constitutive law of the steel tubes in concrete-filled steel tube (CFT) columns, experimental research and full-range elastic-plastic analysis on the nonlinear mechanical behavior of CFT stub columns have been conducted, and the experimental and analytical results are presented in this paper.

Eleven circular CFT stub columns were fabricated and tested under monotonic axial compression, covering the concrete strength from 40MPa to 79MPa and the diameter-to-thickness (D/t) ratio of the steel tubes from 31 to 115. Based on the measured strain histories of the steel tubes and the so-called total deformation theory of plasticity, the stress paths of 99 measured points on the surface of the steel tubes were obtained and analyzed.

Analysis of the stress path governed by Mises yield and isotropic hardening criteria has indicated that (1) with increasing D/t, the steel tube is more likely to yield axially before it gets into biaxial stress state, and as the D/t ratio exceeds 93, the steel tube does yield longitudinally before entering biaxial stress state; (2) deformation of the steel tube exhibits a decreasing trend from the top section to the bottom section along the column height; and (3) the average vertical yield stress of steel tube in CFT is about 0.88 of the steel yield stress f_{sy} and the corresponding hoop stress that will confine the core concrete is about $0.21f_{sy}$.

In addition, an approach to obtaining the full-range axial stress-strain curve of steel tube considering the effects of the biaxial stress state and local buckling was proposed. This method integrating the total deformation theory of plasticity and experimental data involved in modifying the constitutive model of circular hollow steel (CHS) tubes proposed by the authors from uniaxial compressive stress state to biaxial stress state. To verify the validity of the proposed method, the full-range axial load-carrying capacities of the specimens were calculated by superposing the axial load capacities of confined concrete and steel tube. The load-carrying capacities of the confined concrete and the steel tube were obtained by employing the widely used Sakino-Sun's concrete model and the proposed method for steel tubes of CFT, respectively. It has been found that the calculated results are in satisfactory agreement with the experimental load-strain curves, which implies the rationality of this method to adequately reflect the effect of local buckling and lateral dilation of the filled concrete on the axial behavior of steel tubes. Besides, the calculated results also have revealed that the infilled concrete has little, if any, effect on the ascending portion of the compressive stress-strain curves of the steel tubes.

Keywords: concrete-filled steel tube; composite action; full-range elastic-plastic analysis; stress path; stress-strain curve

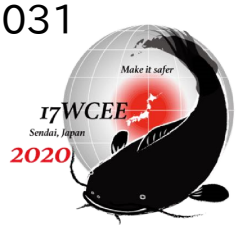

1. Introduction

Concrete filled steel tube (CFT) has widespread applications in high-rising buildings, deep underground tunnels and bridge piers as the main gravity-sustaining and earthquake-resisting components. Lateral confinement provided by the steel tube on the core concrete contributes to the enhancement of the load-carrying capability, stiffness and ductility of the CFT columns. To clarify the interaction between the steel tube and the core concrete, extensive experimental and numerical researches have been conducted on CFT columns. The effect of critical parameters, such as the concrete strength [1-6], the yield strength of steel tube [2-3], and the diameter-to-thickness ratio D/t [2, 5-7], has been explored on the mechanical performance of the CFT. However, the quantitative evaluation of the interactive effect on the CFT columns still remains to be a difficult problem. As a widely used solution to this problem, the method of superposition aims at respectively investigating the mechanical behavior of confined core concrete and biaxially stressed steel tube of CFT.

A survey on the confined concrete under a multiaxial stress state has been conducted by hydrostatic pressure test on cylindrical concrete specimens since 1928 [8]. For decades, considerable experimental data on the confined concrete covering a wide range of concrete strength and confining stress has been published in literature [9-11]. Based on the experimental database, numerous analytical models of mathematical function have been built up for the stress-strain relationship of the concrete confined by spirals, ties and steel tube [12].

However, the limited focus has been put on the survey to clarify the nonlinear mechanical performance of the steel tube of CFT. At present, two strategies have been applied in existing literature to achieve this goal. One approach is based on the incremental Prandtl-Reuss theory to obtain the elastic-plastic relation of the steel tube of CFT. This method has been verified reliable [13-14], but its iterative calculation procedure is complex for practical application. Another method is the experimental and analytical investigation on the mechanical performance of the hollow steel tube (CHS) [15-18]. By this means, the local buckling effect on the load-carrying capability has been clarified, but the effect produced by the core concrete on the behavior of the steel tube has been ignored. When it comes to the design and analysis work of the structures involving in CFT elements, the existing stress-strain models for the steel tube of CFT, such as the elastic-perfectly plastic relation with reduced yield stress by Sakino et al. [19] and Lai et al. [20], bilinear model with hardening branch by Hatzigeorgiou et al. [21] and model of steel material with strain-hardening by Zhong et al. [22], cannot fully reflect the biaxial stress state and the local buckling effect. It is urgent to develop an efficient method to have a deep understanding of the nonlinear behavior of the steel tube.

To fill this gap, experimental and elastic-plastic analysis work on the steel tube of CFT was presented in this paper. Eleven circular CFT stub columns were fabricated and tested under uniaxial compression with concrete strength ranging from 40MPa to 79MPa and the diameter-to-thickness (D/t) ratio of the steel tubes varying from 31 to 115. Nine paired vertical and hoop strain distributed on the exterior surface of the steel tube of each specimen were measured by strain gauges. The total deformation theory of plasticity was applied to interpret the measured strain history into the stress path, which was governed by Mises yield and isotropic hardening criteria. In view of the obtained stress path, the stress transmitting pattern and the relationship between the D/t ratio and the occurrence of the biaxial stress state and local buckling were analyzed. Moreover, an approach of elastic-plastic analysis to obtain the full-range axial stress-strain relation of steel tube was proposed. This method incorporates the total deformation theory of plasticity and the measured strain history of the specimens to find out the relationship of the axial stress between the CHS and the steel tube of CFT. Based on the obtained relationship, the full-range stress-strain relation of the steel tube of CFT was obtained by modifying the stress-strain model of CHS by Sun et al. [23], which was verified reliable.

2. Experimental Research

2.1 Column specimens

Eleven CFT stub column specimens were manufactured using the cold-formed circular steel tube with yield stress f_{sy} of 305MPa, 312MPa, 329MPa and 429MPa. The length-to-outer diameter L/D of the specimens was specified as 3 to avoid the end-constraint effect of stub columns with minimum effect from slenderness. The diameter-to-thickness ratio D/t was varying from 31 to 115. The generalized diameter-to-thickness ratio of the steel tube, introduced in the form of $\alpha=Df_{sy}/tE_s$ [24], was covering from 0.06 to 0.17. The compressive 28-day

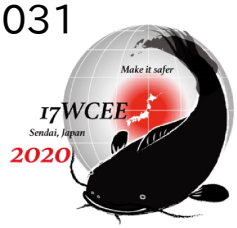

strength $f_{c,28}$ of the standard concrete cube with a dimension of 150mm×150mm×150mm [25] was 33MPa, 40MPa and 54MPa. On the day of test, the compressive strength $f_{c,test}$ of the standard concrete cube was 40MPa, 53MPa and 79MPa.

Table 1 – Critical parameters of the specimens

Specimens	D (mm)	t (mm)	f_{sy} (MPa)	$f_{c,28}$ (MPa)	$f_{c,test}$ (MPa)	$f_{cu,k}$ (MPa)	$f_{cu,kcy}$ (MPa)	α
CFT-31-C60	219	7.06	429	40	53	70	60	0.06
CFT-31-C80	219	7.06	429	54	79	93	81	0.06
CFT-55-C30	273	5.00	312	33	40	58	50	0.08
CFT-55-C60	273	5.00	312	40	53	70	60	0.08
CFT-55-C80	273	5.00	312	54	79	93	81	0.08
CFT-78-C30	273	3.50	305	33	40	58	50	0.12
CFT-78-C60	273	3.50	305	40	53	70	60	0.12
CFT-78-C80	273	3.50	305	54	79	93	81	0.12
CFT-93-C30	325	3.57	329	33	40	58	50	0.15
CFT-93-C60	325	3.57	329	40	53	70	60	0.15
CFT-125-C30	376	3.28	305	33	40	58	50	0.17

The template of the standard cube was taken off 24 hours after casting, while the steel tube of specimens sustainably served as the template to the core concrete. The humid curing environment inside the steel tube with a low coefficient of contraction and slow shrinkage would result in a higher strength of the core concrete than the standard concrete cube. If the curing duration is short, the strength difference caused by the different dismantling template time can be ignored. But the curing duration of this test lasted more than one year, the strength difference between the core concrete and standard concrete cube was likely to be obvious according to the maturity theory. Thus, the compressive strength $f_{c,test}$ should be further modified based on the concept of maturity M_l (^oCd) to reflect the strength $f_{cu,k}$ of core concrete on the test day. The calculation method is presented by Eq. (1)-(3) according to the research [26]. Maturity M_l (^oCd) of the core concrete confined by steel tube can be expressed by Eq. (1). The strength $f_{cu,l}$, the ratio of $f_{cu,k}$ to $f_{c,28}$ in percentage, can be calculated by Eq. (2).

$$M_l = \sum k_i \, (T_i + 10) t_i \tag{1}$$

$$f_{cu,l} = 27.4 M_l^{0.1923} \tag{2}$$

$$f_{cu,k} = \frac{f_{cu,l} \times f_{c,28}}{100} \tag{3}$$

Where t_i (d) is the curing duration, which is 492 days in this experiment. T_i (^oC) is the curing temperature, of which average value is 20^oC during the curing duration. k_i is the coefficient of temperature and adopted as 1.

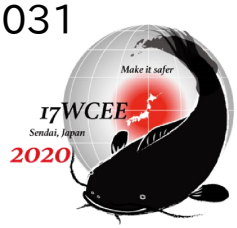

To transform the compressive strength $f_{cu,k}$ of the standard concrete cube to corresponding concrete cylinder strength $f_{cu,kcy}$ with diameter 100mm×height 200mm, the following Eq. (4) is adopted [27]. The details of all the critical parameters are summarized in Table 1.

$$f_{cu,kcy} = \frac{0.8513 f_{cu,k} - 1.5998}{0.96} \tag{4}$$

2.2 Test arrangements and measurements

The specimens were tested under uniaxial compression by a servo-controlled hydraulic machine. The test layout and instrumentation location are shown in Fig. 1. Four electronic displacement transducers (LVDTs) were placed to monitor the axial deformation of the specimens. Paired vertical and horizontal strain gauges placed at nine points of the steel tube surface respectively measured the axial deformation and perimeter expansion of the steel tube.

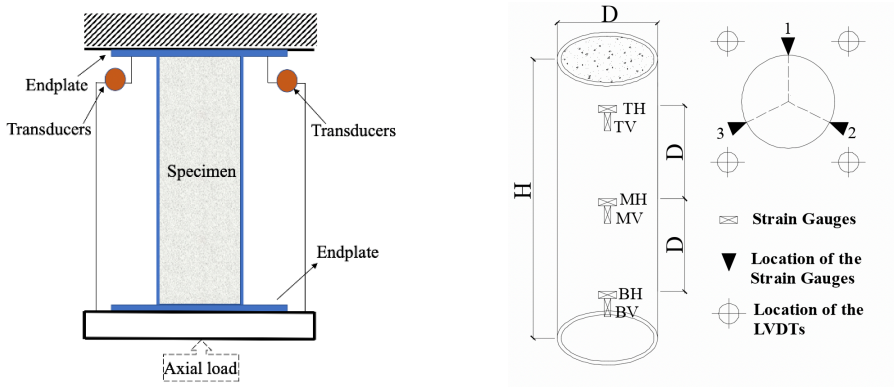

Fig. 1 – Test layout and instrumentation location

3. Theoretical analysis

At the initial loading stage, expansion of the steel tube develops faster than the core concrete. With increasing deformation, the interaction between the core concrete and steel tube occurs due to the Poisson's ratio of concrete exceeds that of the steel tube. Since then, the steel tube is biaxially stressed. To interpret the information of the interaction from test results, the total deformation theory of plasticity is applied, which essentially follows the content of the literature [28].

As shown in Fig. 2, the principal stress σ_1, σ_2 and σ_3 with corresponding strain ε_1, ε_2 and ε_3 of the cubic element of steel tube follow the Hook's law by Eq. (5)-(7) at the elastic stage. The Poisson's ratio ν is assumed to be 0.3 at this stage.

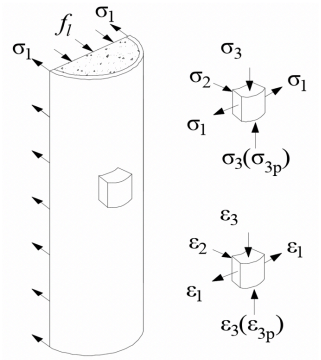

Fig. 2 –Stress components of steel tube

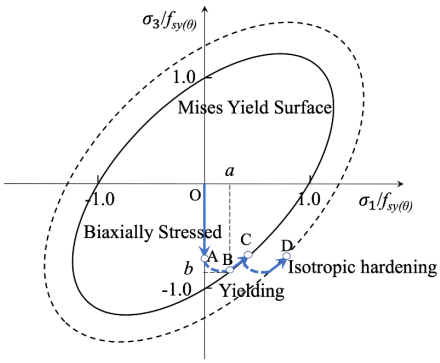

Fig. 3 –Yield criteria and flow rules of steel tube

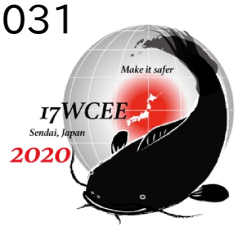

$$\varepsilon_1 = \frac{1}{E}[\sigma_1 - \nu(\sigma_2+\sigma_3)] \quad (5)$$

$$\varepsilon_2 = \frac{1}{E}[\sigma_2 - \nu(\sigma_1+\sigma_3)] \quad (6)$$

$$\varepsilon_3 = \frac{1}{E}[\sigma_3 - \nu(\sigma_1+\sigma_2)] \quad (7)$$

At the plastic stage, the relationship between octahedral shear stress τ_{oct} and the equivalent stress $\bar{\sigma}$ can be expressed by Eq. (8)-(9).

$$\tau_{oct} = \frac{1}{3}\sqrt{(\sigma_1 - \sigma_2)^2 + (\sigma_2 - \sigma_3)^2 + (\sigma_1 - \sigma_3)^2} \quad (8)$$

$$\tau_{\mathrm{oct}} = \frac{\sqrt{2}}{3}\bar{\sigma} \quad (9)$$

To reflect the relationship of the vertical and hoop stress, α_1, α_2 and α_3 are defined as the ratios of principle stress by Eq. (10). Thus, the τ_{oct} can be simplified by Eq. (11).

$$\alpha_1 = \sigma_1/\sigma_3, \quad \alpha_2 = \sigma_2/\sigma_3, \quad \alpha_3 = \sigma_3/\sigma_3 \quad (10)$$

$$\tau_{\mathrm{oct}} = \frac{\sqrt{2}}{3}\sigma_3\sqrt{{\alpha_1}^2 + {\alpha_2}^2 + 1 - \alpha_1\alpha_2 - \alpha_1 - \alpha_2} \quad (11)$$

At axial stress state (α_1=0, α_2=0, α_3=1), the octahedral shear stress $\tau_{oct,a}$ can be expressed by Eq. (12), while for the octahedral shear stress $\tau_{oct,b}$ of biaxial stress state (α_2=0, α_3=1), it can be obtained by Eq. (13). The σ_{3a} and σ_{3b} are respectively the axial stress of steel under axial and biaxial stress circumstances.

$$\tau_{\mathrm{oct,a}} = \frac{\sqrt{2}}{3}\sigma_3 = \frac{\sqrt{2}}{3}\sigma_{3\mathrm{a}} \quad (12)$$

$$\tau_{\mathrm{oct,b}} = \frac{\sqrt{2}}{3}\sigma_3 = \frac{\sqrt{2}}{3}\sigma_{3b}\sqrt{{\alpha_1}^2 + 1 - \alpha_1} \quad (13)$$

The yield and flow rules are assumed to follow the Von Mises and Isotropic Hardening criterions as illustrated in Fig. 3. Octahedral shear stress τ_{oct} is independent of stress state and only related to the principal stress. That is, equivalent stress determines the yield of steel no matter in what stress state as expressed in Eq. (14).

$$\tau_{\mathrm{oct,a}} = \tau_{\mathrm{oct,b}} \quad (14)$$

Substituting Eq. (12) and (13) into Eq. (14), the relationship of axial stress of steel in axial and biaxial condition is obtained by Eq. (15). The reduction factor for the axial stress of steel tube from axial to biaxial stress state is defined as ψ in Eq. (16).

$$\sigma_{3b} = \sigma_{3a}/\sqrt{{\alpha_1}^2 + 1 - \alpha_1} \quad (15)$$

$$\psi = 1/\sqrt{{\alpha_1}^2 + 1 - \alpha_1} \quad (16)$$

Based on the assumption that the components of deviatoric stress and strain are proportional, Eq. (17) can be obtained. μ' is a function of the strain state.

$$\frac{\sigma_1-\sigma_2}{\varepsilon_1-\varepsilon_2} = \frac{\sigma_2-\sigma_3}{\varepsilon_2-\varepsilon_3} = \frac{\sigma_3-\sigma_1}{\varepsilon_3-\varepsilon_1} = 2\mu' \quad (17)$$

If the assumptions that (1) the equivalent stress $\bar{\sigma}$ is a function of the equivalent strain $\bar{\varepsilon}$ as Eq. (18), and (2) the volume of steel is incompressible (Poisson's ratio ν=0.5) are valid, the μ' can be calculated by Eq. (19). E' is a function of the equivalent strain and stress.

$$\overline{\sigma} = E'\overline{\varepsilon} \tag{18}$$

$$\mu' = \frac{E'}{2(1+\upsilon)} = \frac{E'}{3} \tag{19}$$

Incorporating Eq. (17) and Eq. (19), the relation of the principal stress and strain at plastic stage can be expressed as Eq. (20)-(22). For simplicity, β_1, β_2 and β_3 are the ratio of principal strain defined by Eq. (23).

$$\varepsilon_1 = \frac{1}{E'}\left[\sigma_1 - \frac{1}{2}(\sigma_2+\sigma_3)\right] \tag{20}$$

$$\varepsilon_2 = \frac{1}{E'}\left[\sigma_2 - \frac{1}{2}(\sigma_1+\sigma_3)\right] \tag{21}$$

$$\varepsilon_3 = \frac{1}{E'}\left[\sigma_3 - \frac{1}{2}(\sigma_1+\sigma_2)\right] \tag{22}$$

$$\beta_1 = \varepsilon_1/\varepsilon_3,\ \ \beta_2 = \varepsilon_2/\varepsilon_3,\ \ \beta_3 = \varepsilon_3/\varepsilon_3 \tag{23}$$

For the steel tube of CFT, β_2=0 in biaxial stress state and β_1 can be calculated by the measured strain history. Substituting Eq. (10) and Eq. (23) into Eq. (5)-(7) and Eq. (20)-(22), the α_1 at the elastic and plastic stage can be calculated respectively by Eq. (24) and Eq. (25). Thus, the relationship of axial stress of steel in axial and biaxial stress state as Eq. (15) can be calculated.

$$\alpha_1 = \frac{\beta_1+0.3}{1+0.3\beta_1} \tag{24}$$

$$\alpha_1 = \frac{\beta_1+0.5}{1+0.5\beta_1} \tag{25}$$

The stress path of the steel assumed to follow the Mises yield and isotropic hardening criterion can be obtained by Eq. (26)-(27). Where the f_{sy} and $f_{sy\theta}$ represent the yield stress of initial yield surface and isotropic hardening surface respectively.

$$\frac{\sigma_3}{f_{sy}} = \frac{1}{\sqrt{\alpha_1^2-\alpha_1+1}} \text{ or } \frac{\sigma_3}{f_{sy\theta}} = \frac{1}{\sqrt{\alpha_1^2-\alpha_1+1}} \tag{26}$$

$$\frac{\sigma_1}{f_{sy}} = \frac{\alpha_1}{\sqrt{\alpha_1^2-\alpha_1+1}} \text{ or } \frac{\sigma_1}{f_{sy\theta}} = \frac{\alpha_1}{\sqrt{\alpha_1^2-\alpha_1+1}} \tag{27}$$

4. Experimental results

4.1Ratios β_1 of hoop strain to vertical strain of the measured point

Ratios β_1 of hoop strain to axial strain of the monitored points by strain gauges are presented in Fig. 4. The $\beta_{T\text{-}ave}$, $\beta_{M\text{-}ave}$ and $\beta_{B\text{-}ave}$ are respectively the average $\beta_1$of three measured points distributed across the section from top to bottom of the specimens if the assumption of plane-remain-plane is valid.

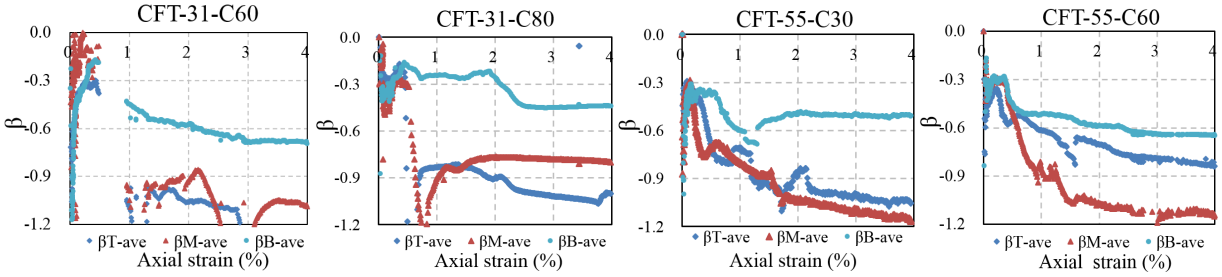

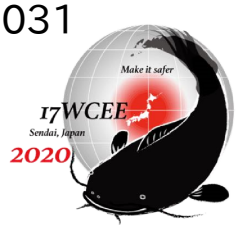

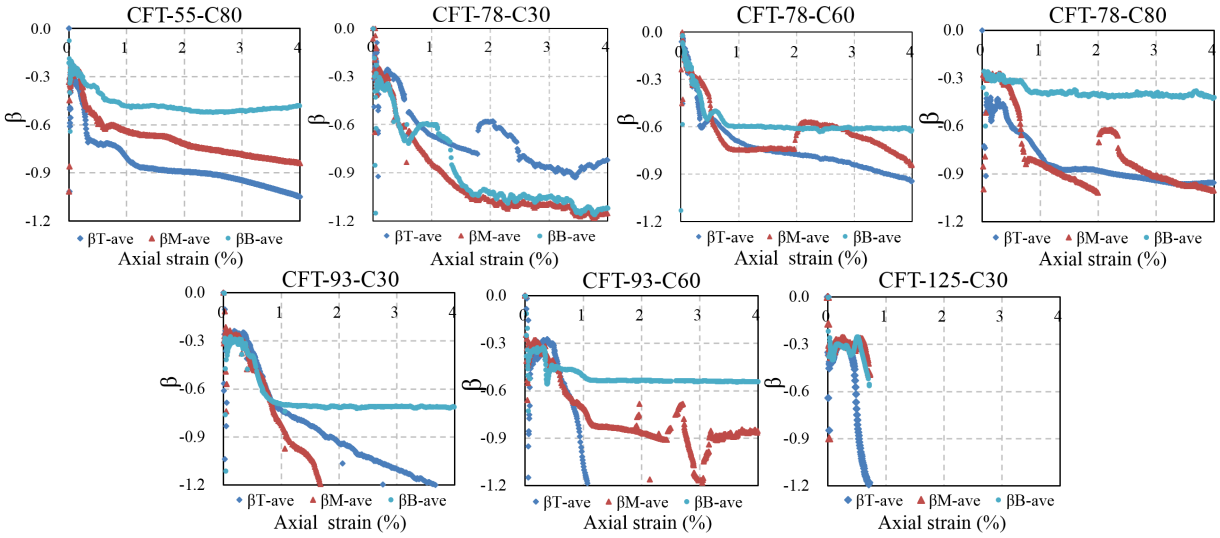

Fig. 4– Ratios β1 of hoop strain to vertical strain

It indicates that the Poisson's ratio of the steel tube is about 0.3 at the elastic stage. With increasing longitudinal deformation, nearly all the ratios $\beta_{T\text{-}ave}$ and $\beta_{M\text{-}ave}$ develops faster than $\beta_{B\text{-}ave}$. It reveals that the dilation of core concrete has little impact on the bottom part of the steel tube and the performance of the upper-region steel tube is of representative to reflect the local buckling effect and biaxial stress state. Therefore, ratio β_1 in the following calculation will be taken as the average value of $\beta_{T\text{-}ave}$ and $\beta_{M\text{-}ave}$.

4.2 Stress paths of the measured points

Substituting the obtained average value of $\beta_{T\text{-}ave}$ and $\beta_{M\text{-}ave}$ into the Eq. (24)-(25), the stress development of the steel tube within the middle and upper region of the specimens is calculated according to the Eq. (26)-(27).

As shown in Fig. 5, the stress paths of the steel tube reveal that the steel tube is axially stressed at the initial loading stage. With increasing deformation, the steel tube starts to be biaxially stressed and since then, the core concrete is confined by the steel tube. When the stress path reaches the yield surface, the steel tube yields with reduction yield stress compared with the uniaxial stressed steel. After that, the stress flows to the isotropic hardening surface, which can be clearly reflected by the specimens of CFT-55-C80, CFT-78-C60, CFT-78-C80, CFT-93-C30 and CFT-93-C60.

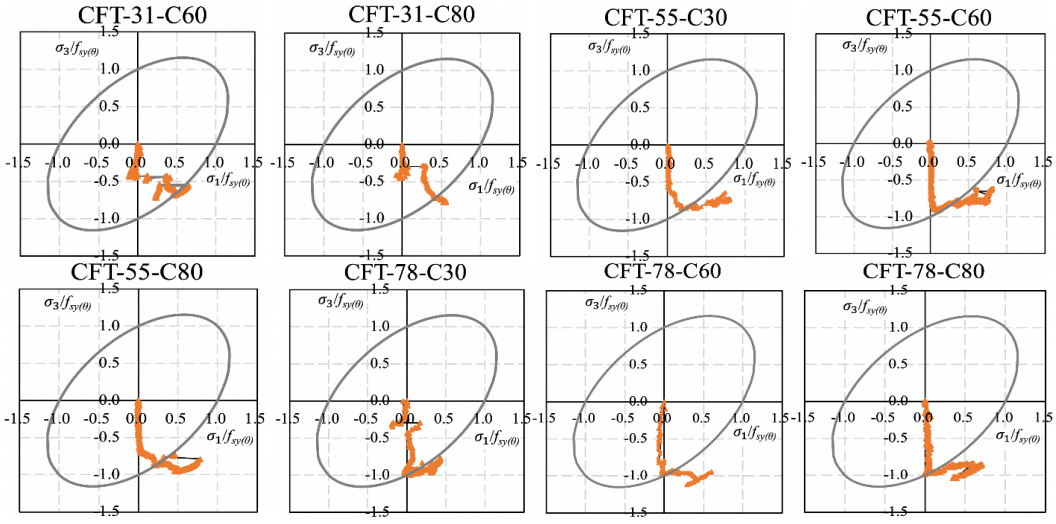

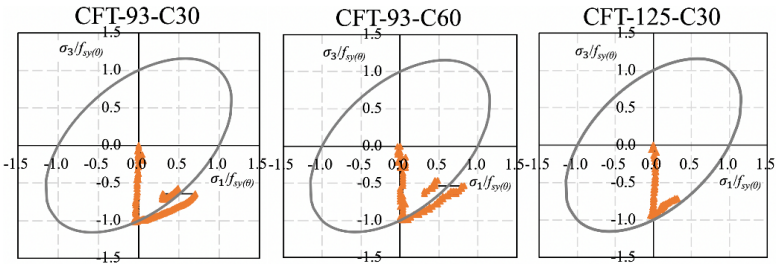

Fig. 5–Stress paths of the steel tube

4.3 Vertical yield stress of steel tube of CFT

Comparing with the axially stressed steel, the vertical yield stress of the biaxially stressed steel is reduced. To quantify the reduction of vertical yield stress caused by biaxial stress state, coordinates (a, b) of the yield point B in Fig. 3 are collected in Fig. 6. The b_{Tave}, b_{Mave} and b_{Bave} respectively are the average b of three measured points distributed across the cross-section within the top, middle and bottom region of the specimens. The b_{TMave} is the average value of the b_{Tave} and b_{Mave}. It exhibits that (1) with increasing D/t, the steel tube is more likely to yield axially before it gets into biaxial stress state, and as the D/t ratio exceeds 93, the steel tube does yield longitudinally before entering biaxial stress state, and (2) the average vertical yield stress of steel tube in CFT is about 0.88 of the steel yield stress f_{sy} and the corresponding hoop stress providing to core concrete is of 0.21 f_{sy}.

4.4 Reduction factors ψ

Reduction factors ψ can be calculated by Eq. (16) based on the obtained ratios β_1. Typical calculation results of the real-time reduction factor ψ are presented in Fig. 7. The specimens of CFT-31-C80 and CFT-55-C30 are randomly selected. Symbols of rhombus and triangle respectively stand for the average reduction factors $\psi_{T\text{-}ave}$ and $\psi_{M\text{-}ave}$ within the top and middle region of the columns, and the dotted line $\psi_{TM\text{-}ave}$ averaging them is applied to calculate the stress-strain curves of the steel tube of the specimens in the following chapter. It can be seen from Fig. 7 the reduction factors ψ maintains as 1 at the initial stage, which indicates that the axial stress of steel tube in CFT will not be reduced before the interaction occurs.

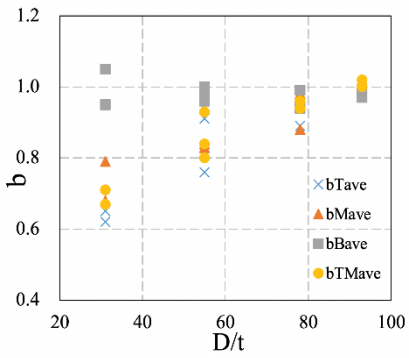

Fig. 6 – Relationship of b and D/t

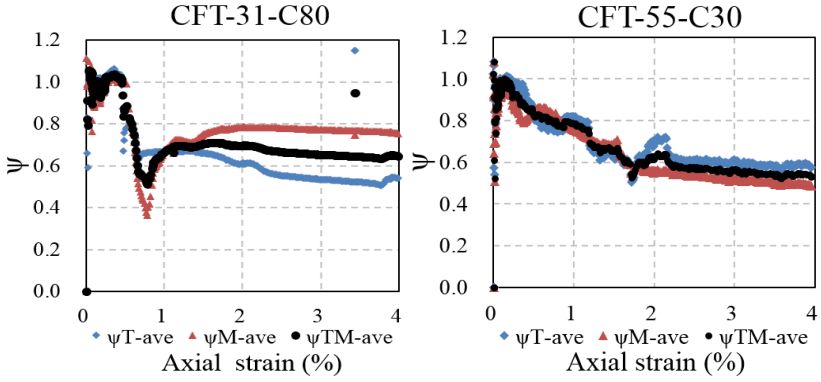

Fig. 7 – Reduction factor ψ

5. Stress-strain curves of the steel tube of the specimens

Sun et al. have proposed a reliable model to predict the stress-strain curve of CHS stub columns, which consists of ascending and descending branches (see Appendix) [23]. The descending branch is to depict the effect of local buckling. However, due to the appearance of infilled concrete, the CHS model cannot be used to investigate the performance of the steel tube of CFT. To obtain the stress-strain curves of the steel tube of the specimens, a method integrating the existing CHS model and experimental database of factor ψ is proposed in this paper as shown in Fig. 8(a).

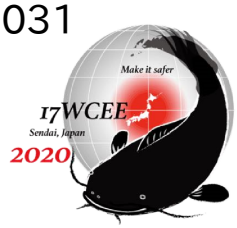

The model of CHS without considering the local buckling is adopted and multiplied by real-time reduction factor ψ to reflect the experimental information of local buckling and biaxial stress state. The obtained typical stress-strain relation of the steel tube of the specimens CFT-31-C80 and CFT-55-C30 are given in Fig. 8(b). The consistent ascending portion of the CHS and the steel tube of CFT at the initial stage indicates that the filled concrete has little, if any, effect on the ascending portion of the constitutive curve of steel tubes.

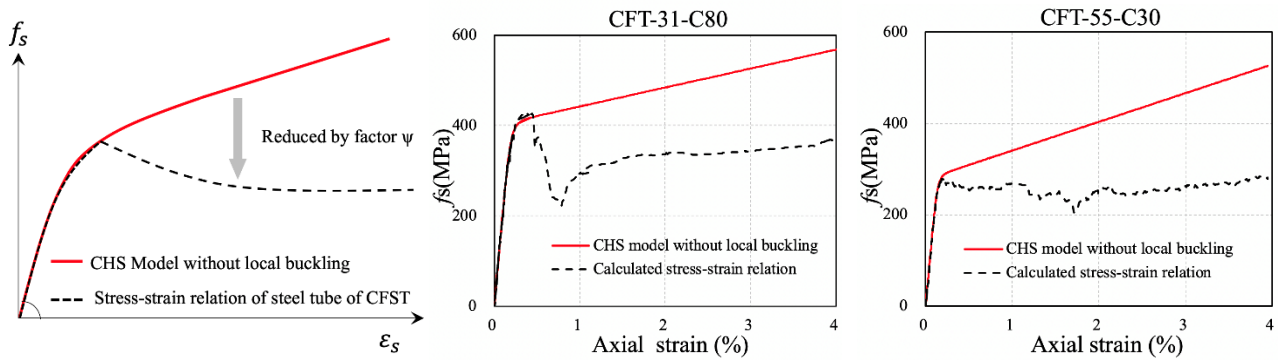

(a) Calculation procedure of the proposed method (b) Calculation results of the stress-strain curve

Fig. 8 –Stress-strain curve of the steel tube of the specimens

6. Verification of the proposed method

To verify the reliability of this proposed method, the non-dimensional calculated N_{cal}/N_0-ε and experimental N_{exp}/N_0-ε load-strain curves of the specimens are compared in Fig. 9. The N_{cal} is the superposition results of the load-carrying capability of steel tube and confined concrete, which can be expressed by Eq. (28). N_c of confined concrete is predicted by Sakino-Sun's model (see Appendix). N_0 is the nominal squash load given by Eq. (29). f_c and f_s are axial stress of the confined concrete model and CHS model corresponding to any axial strain ε_c and ε_s, respectively. A_c and A_s are the cross-section area of the core concrete and steel tube respectively.

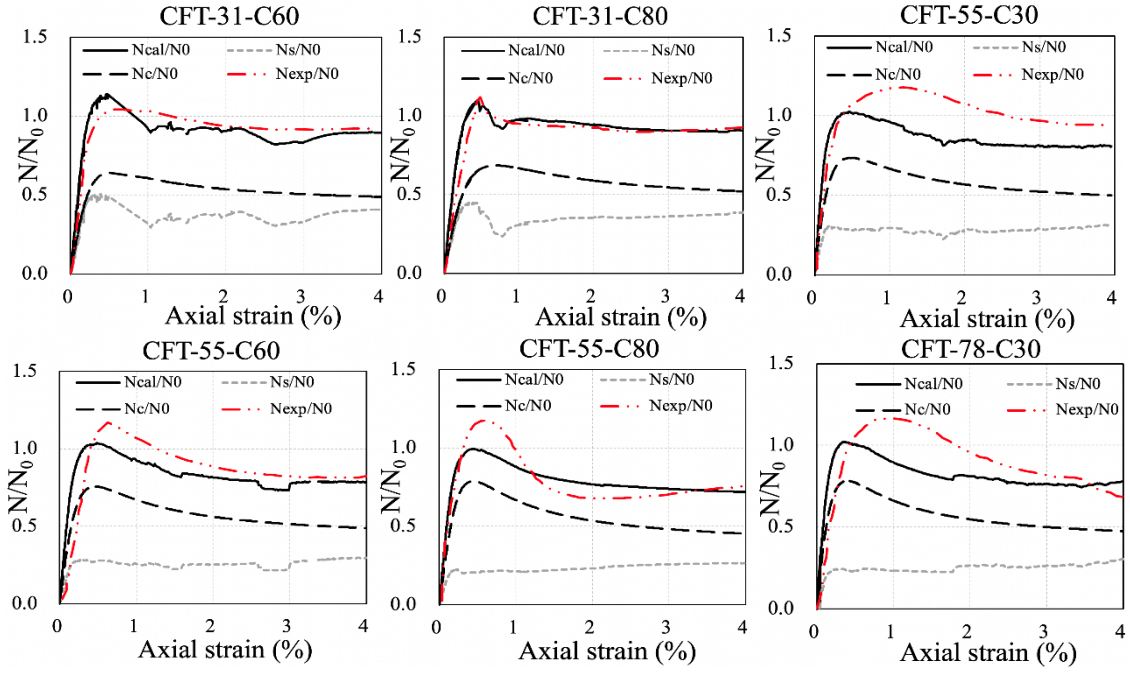

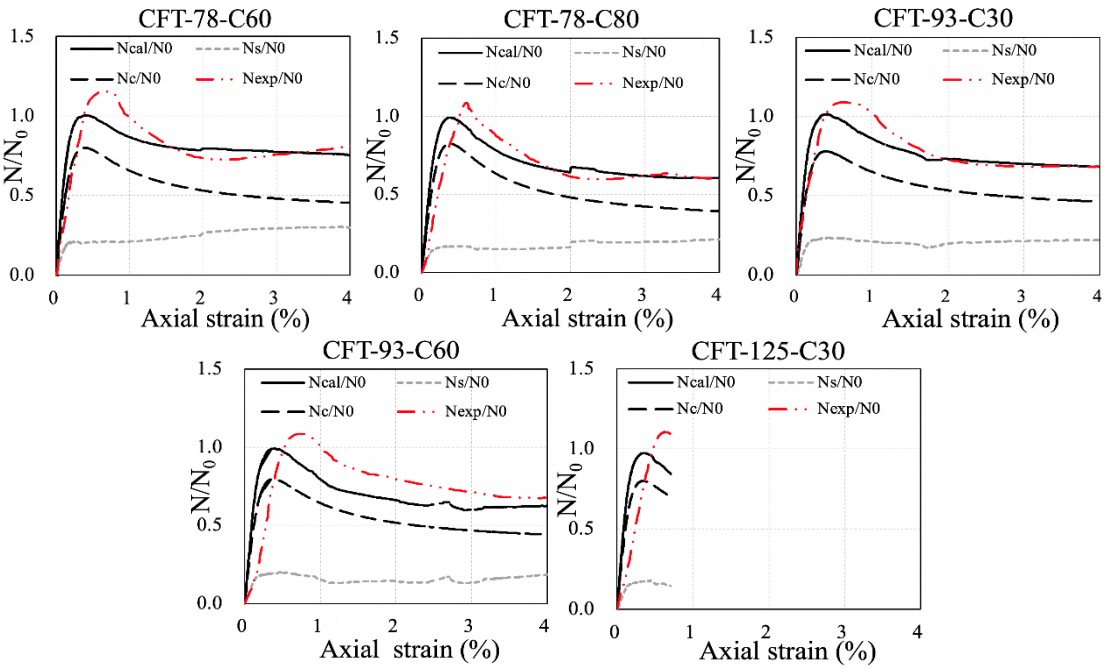

Fig. 9 –Comparisons between the calculated and experimental results

$$N_a = N_c + N_s = A_c f_c + A_s \psi f_s \tag{28}$$

$$N_0 = A_c f_{cu,kcy} + A_s f_{sy} \tag{29}$$

As shown in Fig. 9, satisfactory agreement of the calculated and experimental results verifies the validity of the proposed elastic-plastic analysis method to investigate the mechanical behavior of the steel tube in CFT up to large strain. And the load sharing pattern of the specimens reveals that the steel tube with increasing D/t will be burden with decreasing compressive loadings.

7. Conclusions

Test results of eleven CFT stub columns under concentric compressive loadings have been presented in this paper. The measured strain histories of the steel tubes convey important information regarding to the biaxial stress state and local buckling of them. To interpret this information for a deep understanding of the performance of the bi-axially stressed steel tubes, an elastic-plastic analysis method has been proposed. The concept of this method is to incorporate the total deformation theory of plasticity with the measured strain history of the steel tube to evaluate the strength reduction of the CHS caused by the multi-axis stress state as well as the local buckling at large strain. Through the elastic-plastic analysis on the test results and the assessment of the proposed method, the following conclusions can be drawn:

(1) Circular steel tube is more likely to yield axially before it gets into biaxial stress state with increasing D/t ratio. When the D/t ratio exceeds 93, the steel tube tends to yield longitudinally before entering a bi-axial stress state.

(2) The average axial yield stress of steel tube in CFT is about 0.88 of the yield strength f_{sy} of the steel, and the corresponding hoop stress providing confinement to the core concrete is about 0.21 f_{sy}.

(3) Deformation of the steel tube exhibits a decreasing trend from the top section to the bottom section along the column height;

(4) The filled concrete has little, if any, effect on the ascending portion of the stress-strain curve of steel tubes.

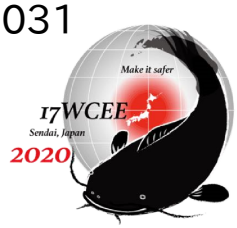

(5) The proposed method is proved to be reliable to obtain the full-range stress-strain relation of the steel tube of circular CFT stub columns and can take account of the effects of the local buckling and biaxial stress state on the stress-strain curves.

7. Acknowledgements

Partially financial supports by the National Key R&D Program of China (2018YFC1504905), the Scientific Research Foundation of the Education Department of Sichuan Province, China (2019YJ0466) and SKLGP open funding (SKLGP2018K021) are greatly appreciated.

8. Appendix

Model	CHS model [23]	Confined concrete model [29]
Figures	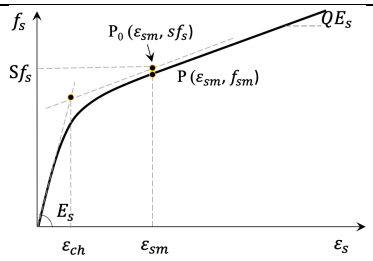	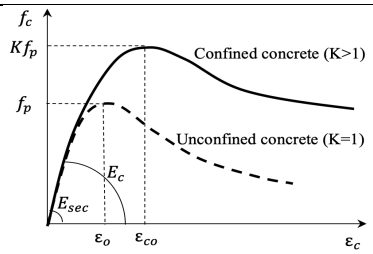
Expressions	$f_s = E_s\varepsilon_s\left(Q + \frac{1-Q}{(1+\lvert\varepsilon_s/\varepsilon_{ch}\rvert^N)^{1/N}}\right)$	$f_c = Kf_p\frac{aX+(b-1)X^2}{1+(a-2)X+bX^2}$

9. References

[1] Yu Z W, Ding F X, Cai C S (2007): Experimental behavior of circular concrete-filled steel tube stub columns. Journal of Constructional Steel Research, 63(2), 165-174.

[2] Ekmekyapar, Al-Eliwi B J M (2016): Experimental behaviour of circular concrete filled steel tube columns and design specifications. Thin-Walled Structures, 105:220-230.

[3] Dundu M (2012): Compressive strength of circular concrete filled steel tube columns. Thin-Walled Structures, 56:62-70.

[4] Oliveira W L A D, Nardin S, Ana Lúcia H. de Cresce El Debs (2009): Influence of concrete strength and length/diameter on the axial capacity of CFT columns. Journal of Constructional Steel Research, 65(12):2103-2110.

[5] Abed F, AlHamaydeh M, Abdalla S (2013): Experimental and numerical investigations of the compressive behavior of concrete filled steel tubes (CFSTs). Journal of Constructional Steel Research, 80: 429-439.

[6] Giakoumelis G, Lam D (2004): Axial capacity of circular concrete-filled tube columns. Journal of Constructional Steel Research, 60(7):1049-1068.

[7] Guler S, Copur A, Aydogan M (2013): Axial capacity and ductility of circular UHPC-filled steel tube columns. Magazine of Concrete Research, 65(15): 898-905.

[8] Richart F E, Brandtzaeg A, Brown R L. (1928): A Study of the Failure of Concrete under Combined Compressive Stresses. University of Illinois, Engineering Experimental Station, Bulletin, 1928.

[9] Gardner N J (1969): Triaxial behavior of concrete. Journal Proceedings, 66(2): 136-158.

[10] Sfer D, Carol I, Gettu R (2002): Study of the Behavior of Concrete under Triaxial Compression. Journal of Engineering Mechanics, 128(2):156-163.

[11] Ansari F, Li Q (1998): High-strength concrete subjected to triaxial compression. Materials Journal, 95(6): 747-

[12] Mander J B, Chang G A (1994): Seismic Energy Based Fatigue Damage Analysis of Bridge Columns: Part 1 - Evaluation of Seismic Capacity. Technical Report.

[13] Lai M H, Ho J C M (2016): A theoretical axial stress-strain model for circular concrete-filled-steel-tube columns. Engineering Structures, 125: 124-143. MLA

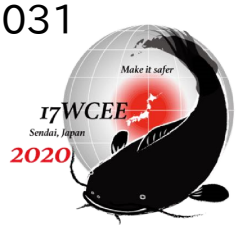

[14] Lin B Z (1990): Research on the circular transversely confined concrete under uniaxial compression. Dissertation, Kyushu University.

[15] M.D. O' Shea, R.Q. Bridge (1997): Local buckling of thin-walled circular steel sections with or without internal restraint. Journal of Constructional Steel Research, 41(2-3):137–157.

[16] M. Elchalakani, X.L. Zhao, R. Grzebieta (2002): Tests on concrete filled double-skin (CHS outer and SHS inner) composite short columns under axial compression. Thin-Walled Structures, 40(5):415–441.

[17] X.L. Zhao, R. Grzebieta, M. Elchalakani (2002): Tests of concrete-filled double skin CHS composite stub column. Steel Composite Structures, 2(2):129–146.

[18] Fujimoto T, Mukai A, Nishiyama I (1997): Axial compression behavior of concrete filled steel tubular stub columns using high strength materials. J. Struct. Constr. Eng., AIJ, 1997 (498): 161-168.

[19] Sakino K, Nakahara H, Morino S (2004): Behavior of centrally loaded concrete-filled steel-tube short columns. Journal of Structural Engineering, 130(2): 180-188.

[20] Lai Z, Varma A H (2016): Effective stress-strain relationships for analysis of noncompact and slender filled composite (CFT) members. Engineering Structures, 124:457-472.

[21] Hatzigeorgiou G D (2008): Numerical model for the behavior and capacity of circular CFT columns, Part I: Theory. Engineering Structures, 30(6): 1573-1578.

[22] Tao Z, Wang Z B, Yu Q (2003): Finite element modelling of concrete-filled steel stub columns under axial compression. Journal of Constructional Steel Research, 89(5):121-131.

[23] Yang C, Zhao H, Sun Y, Zhao S C (2017): Compressive stress-strain model of cold-formed circular hollow section stub columns considering local buckling. Thin-Walled Structures, 120: 495-505.

[24] Architecture Institute of Japan (AIJ), Design Standard for Steel Structures, Marauzen, Tokyo, 1993 (in Japanese).

[25] Standard for test method of mechanical properties on ordinary concrete, GB/T 50081-2002, China (in Chinese).

[26] Zhang Fuliang (2007): The study of early-dismantling template system and dismantling template time of concrete structures. Tongji University, 14-23 (in Chinese).

[27] Lai M H, Ho J C M (2016): A theoretical axial stress-strain model for circular concrete-filled-steel-tube columns. Engineering Structures, 125: 124-143.

[28] Valluri S R (1966). Fracture under Biaxial Conditions in the Presence of a Crack. ICF1, Japan 1965.

[29] Sun Y P, Sakino K (1998): Modelling for the axial behaviour of high strength CFT columns. Proceedings of the 23rd Conference on our World in Concrete & Structures, Singapore. 25-26. MLA

